Synthesis and Properties of Symmetric Glycerol-Derived 1,2,3-Triethers and 1,3-

Diether-2-Ketones for CO₂ Absorption

Shuai Qian, Xiaoyang Liu, C. Heath Turner & Jason E. Bara*

Department of Chemical & Biological Engineering, University of Alabama, Tuscaloosa, AL,

35487-0203, USA

Corresponding author's email address: <u>jbara@eng.ua.edu</u> (Jason E. Bara)

Abstract

Five compounds bearing glycerol skeletons: 1,3-diethoxypropan-2-one ([E, K, E]),

2,5,9,12-tetraoxatridecan-7-one ([ME, K, ME]), 1,3-bis(2,2,2-trifluoroethoxy)propan-2-one ([F, K,

F]), 7-(2-methoxyethoxy)-2,5,9,12-tetraoxatridecane ([ME, ME, ME]) and 2-(2-methoxyethoxy)-

1,3-bis(2,2,2-trifluoroethoxy)propane ([F, ME, F]) – were synthesized from epichlorohydrin at

molar scales with high regioselectivity. Density and viscosity were measured over a temperature

range of 293.15 to 353.15 K. Henry's constants for CO₂ were obtained under moderate pressures

(2 to 10 atm) at 303.15, 318.15, 333.15 and 348.15 K. Comparison of CO₂ affinity with dimethyl

ethers of polyethylene glycol (DMPEG) and ionic liquids (ILs) indicated that [ME, ME, ME] and [F,

ME, F] are excellent candidates as novel physical solvents for CO₂ capture. DFT calculations were

performed to understand the structure-property-performance relationships for the CO₂

absorption mechanism. All five compounds were miscible with most common solvents except

hexanes and water. In addition to gas absorption applications, these compounds might also find

use as general purpose green solvents.

Keywords: Glycerol, green chemistry, solvents, CO₂ absorption, DFT calculations

1. Introduction

Glycerol is the main byproduct of biodiesel production (10% by weight). Despite of its versatile applications in food, cosmetics, medicine, fuels, etc.,^[1] the supply of glycerol has surged in the past decade. It is estimated that glycerol production outstrips demand by at least 33%,^[2] and the gap is enlarging alongside the growth of biodiesel demand. Therefore, development of new applications where glycerol is used as a feedstock will improve the economics of biofuels and further support the proliferation of renewable fuels. New physical solvents based on glycerol skeletons for CO₂ emission control present one opportunity to utilize glycerol to replace petroleum-derived resources.

Dimethyl ethers of polyethylene glycol (DMPEG) are used as the solvent in the commercial Selexol® process to remove CO₂ from gas streams where CO₂ is present at high concentrations and/or pressures.DMPEG has relatively high absorption capacity, minimal energy cost for heating/refrigerating and solvent regeneration, low viscosity and low vapor pressure. ^[3, 4, 5] Apart from DMPEG, ionic liquids (ILs) have been studied for CO₂ treatment due to their adequate CO₂ capacity, negligible vapor pressure, good thermal stability, etc. although high viscosity is the main obstacle preventing them from broad utilization. ^[6, 7] To avoid the inherent disadvantages of conventional ILs, it is worth considering new molecules with higher CO₂ capacity (i.e., smaller Henry's constants) and lower viscosity. Our prior work indicated that etherified glycerol derivatives might be competitive candidates as novel green solvents for CO₂ capture purpose. ^[8, 9, 10] Apart from ethers, ketones bearing a glycerol skeleton have rarely been studied in the literature, but their facile synthesis and potential applications make this a compelling class of molecules. For example, they could be utilized as replacement intermediates for acetone in the

synthesis of solketal analogues with more ether substitutes. Moreover, there are interesting aspects of the affinity between CO₂ and ketones with enhanced polarity over corresponding alcohols and ethers. This work is intended to develop symmetric ketones and triethers with several different functional groups attached to the ether sites of the glycerol backbone. Information about the molecules synthesized and studied in this work are shown in Table 1.

Epichlorohydrin, a commercially available and value-added product derived from glycerol (i.e., glycerol + 2 HCl -> epichlorohydrin) is used for the synthesis tasks in order to achieve delicate regioselectivity with good yield. Upon successful synthesis of target materials, characterizations of density and viscosity were performed and data were analyzed. CO₂ absorption measurements were then conducted and Henry's constants were interpreted and extrapolated to allow for comparison with other physical solvents. Furthermore, CO₂-solvent interactions were calculated via DFT methods and analyzed by the reduced density gradient (RDG) and independent gradient model (IGM) to understand the absorption process. Finally, the miscibility of these glycerol-derived compounds with common organic solvents and water was tested for general guidance of solvent applications.

Table 1: Names, formulas, structures, acronyms and CAS registry numbers of compounds studied in this work.

Name	Formula	Structure	Acronym/CAS #
1,3-diethoxypropan-2-one	C ₇ H ₁₄ O ₃	\\\\\\\\\\\\\\\\\\\\\\\\\\\\\\\\\\\\\\	[E, K, E] 5460-70-8
2,5,9,12-tetraoxatridecan-7-one	C ₉ H ₁₈ O ₅	000000	[ME, K, ME] 130670-58-5
1,3-bis(2,2,2- trifluoroethoxy)propan-2-one	C ₇ H ₈ F ₆ O ₃	F ₃ C O CF ₃	[F, K, F] N/A
7-(2-methoxyethoxy)-2,5,9,12- tetraoxatridecane	$C_{12}H_{26}O_6$		[ME, ME, ME] 14002-61-0
2-(2-methoxyethoxy)-1,3-bis(2,2,2-trifluoroethoxy)propane	C ₁₀ H ₁₆ F ₆ O ₄	F ₃ C O O CF ₃	[F, ME, F] N/A

2. Experimental

2.1 Materials

Dichloromethane (CH₂Cl₂, 99.5% min), Methanol (MeOH, 99.8% min), Acetone (99.5% min), N,N-Dimethylformamide (DMF, 99.8% min), Ethanol (EtOH, 99% min), Sodium hydroxide (NaOH, 97%) and Sodium bicarbonate (NaHCO₃, 99.7% min) were purchased from VWR; (±)-Epichlorohydrin (99%), 2,2,2-Trifluoroethanol (CF₃CH₂OH, 99%), 2-methoxyethanol (CH₃OCH₂CH₂OH, 99%), 2-Chloroethyl methyl ether (CH₃OCH₂CH₂Cl, 98%), Oxalyl chloride (98%) and Chloroform-d (CDCl₃-d, 99.8% with 1% TMS) were purchased from BeanTown Chemical; Toluene (99.8%) and Sodium (Na, 99%) were purchased from Alfa Aesar; ACS grade tetrahydrofuran (THF) and Hexanes (mixture of isomers) were purchased from Avantor; ACS

grade Dimethyl sulfoxide (DMSO) and anhydrous Magnesium sulfate (MgSO₄, 98.0% min) were purchased from EMD Millipore Corporation; Diethyl ether (Et₂O, anhydrous, 99.0% min) was purchased from J.T. Baker; Triethylamine (Et₃N) was purchased from Oakwood Chemical; DMSO- d_6 (99% with 0.05% V/V TMS) was purchased from Cambridge Isotope Laboratories; HydranalTM (Coulomat AG) was purchased from Honeywell; Molecular sieves (3Å, 3.2 mm pellets) were purchased from Sigma-Aldrich; Deionized water was obtained from a 12 M Ω source in Chemistry Department at the University of Alabama; CO₂ (99.999%) was purchased from Airgas. All chemicals were used without further purification.

2.2 Synthesis

The synthetic routes of the compounds studied in this work are shown in Scheme 1. All reactions were performed at molar scales.

Scheme 1: Synthesis route to symmetric ketones and triethers.

2.2.1 Synthesis of symmetric secondary alcohol compounds [R₁, 0, R₁]

Three symmetric secondary (2°) alcohol compounds - [E, 0, E], [ME, 0, ME] and [F, 0, F] - were synthesized for further modification using different synthesis strategies based on the

nature of corresponding primary alcohols (R_1OH) and the products. Procedures applied were similar to those described in our previous work [9] with optimizations for higher yield.

2.2.1.1 1,3-diethoxypropan-2-ol ([E, 0, E])

To a 1000 mL round bottom flask loaded with 500 mL EtOH at RT was added sodium metal (Na $^{\circ}$) (25.3 g, 1.10 mol). Temperature was raised to 70 °C upon depletion of Na $^{\circ}$, followed by addition of epichlorohydrin (46.7 g, 0.50 mol) dropwise. Reaction was kept overnight at 70 °C before the excess EtOH was removed by rotary evaporation under reduced pressure. 400 mL Et₂O was then added to the crude product and the precipitate was removed by filtration. The solution was then neutralized with 1 M HCl. The mixture was transferred into a 1000 mL separation funnel, where the Et₂O phase was collected and the aqueous phase was further washed with 3 × 100 mL Et₂O. The organic phases were combined and dried over anhydrous MgSO₄. The solids were filtered and solvent was removed by rotary evaporation, followed by vacuum distillation to afford 54.67 g (73.8%) of [E, 0, E] as a clear, colorless liquid. 1 H NMR (500 MHz, DMSO- $^{\circ}$ d₆) δ 4.71 (d, $^{\circ}$ J = 5.2 Hz, 1H), 3.69 (qd, $^{\circ}$ J = 5.8, 5.0 Hz, 1H), 3.47 – 3.39 (m, 4H), 3.33 (dd, $^{\circ}$ J = 9.9, 5.1 Hz, 2H), 3.27 (dd, $^{\circ}$ J = 9.7, 6.0 Hz, 2H), 1.10 (td, $^{\circ}$ J = 7.0, 0.7 Hz, 6H).

2.2.1.2 1,3-bis(2-methoxyethoxy)propan-2-ol ([ME, 0, ME])

To a 1000 mL round bottom flask loaded with 600 mL 2-methoxyethanol (CH₃OCH₂CH₂OH) at RT was added Na⁰ (75.9 g, 3.30 mol). The reaction temperature was raised to 80 °C upon depletion of Na⁰, followed by dropwise addition of epichlorohydrin (140.2 g, 1.50 mol). The reaction was stirred overnight at 80 °C before cooling down to RT. The excess of CH₃OCH₂CH₂OH was removed by rotary evaporation under reduced pressure. 600 mL Et₂O was then added to the

crude product and the precipitate was removed by filtration. The solution was then neutralized with 1 M HCl. The solids were filtered and Et_2O was then removed by rotary evaporation under reduced pressure, followed by vacuum distillation to afford 196.69 g (63.0%) [ME, 0, ME] as a clear, colorless liquid. ¹H NMR (500 MHz, DMSO- d_6) δ 4.74 (d, J = 5.2 Hz, 1H), 3.69 (dp, J = 10.9, 5.2 Hz, 1H), 3.54 – 3.49 (m, 4H), 3.46 – 3.41 (m, 4H), 3.38 (dd, J = 9.9, 5.0 Hz, 2H), 3.32 (dd, J = 10.0, 5.9 Hz, 2H), 3.25 (s, 6H).

2.2.1.3 1,3-bis(2,2,2-trifluoroethoxy)propan-2-ol ([F, 0, F])

To a 1000 mL round bottom flask loaded with 4 M aq. NaOH (300 mL) at RT was added 2,2,2-trifluoroethanol (CF₃CH₂OH, 121.3 g, 1.20 mol) and stirred for 30 min before dropwise addition of epichlorohydrin (46.7 g, 0.50 mol). The reaction system was heated at 80 °C overnight before cooling to RT. The reaction mixture was then transferred to a 1000 mL separation funnel and the bottom organic layer was collected. The aqueous layer was washed with 3 × 100 mL CH₂Cl₂. The organic phases were combined, washed with 3 × 50 mL saturated NaHCO₃ solution, dried over anhydrous MgSO₄ and filtered. The solvent was removed by rotary evaporation under reduced pressure and the remaining product was further purified by vacuum distillation to afford 97.0 g (75.7%) [F, 0, F] as a clear, colorless liquid. 1 H NMR (360 MHz, DMSO- d_6) δ 5.16 (d, J = 5.2 Hz, 1H), 4.10 (d, J = 9.4 Hz, 2H), 4.05 (d, J = 9.4 Hz, 2H), 3.80 (h, J = 5.3 Hz, 1H), 3.58 (qd, J = 10.2, 5.3 Hz, 4H).

2.2.2 Synthesis of symmetric ketones [R₁, K, R₁]

Three symmetric ketones bearing glycerol skeleton were synthesized from the corresponding 2° alcohol obtained earlier using the classic Swern oxidation method while the

workup process differed slightly depending on the miscibility of the compound with water in efforts to maximize the yield.

2.2.2.1 1,3-diethoxypropan-2-one ([E, K, E])

To a 1000 mL round bottom flask loaded with 260 mL CH₂Cl₂ at RT was added oxalyl chloride (40 mL, 0.44 mol). The flask was then placed in a dry ice-acetone cooling bath (-78 °C). DMSO (68 mL, 0.64 mol) mixed with 80 mL CH₂Cl₂ was added slowly over 10 min and maintained for another 10 min until no further gas evolved from the reaction system. Then addition of [E, 0, E] (59.3 g, 0.40 mol) dissolved in 100 mL CH₂Cl₂ occurred over 10 min. The reaction was maintained for another 20 min before quenching with Et₃N (278 mL, 2.00 mol). The cooling bath was removed after 1 h to allow the reaction system to warm to ambient temperature, after which 130 mL deionized water was added. After stirring for 30 min in the presence of water, the mixture was transferred to a 1000 mL separation funnel. The bottom CH₂Cl₂ layer was collected and the aqueous layer was washed with 3×100 mL CH₂Cl₂. The organic layers were combined, washed with 3 × 50 mL saturated NaHCO₃ water solution, dried over anhydrous MgSO₄ and filtered, followed by removal of CH2Cl2 by rotary evaporation under reduced pressure. The remaining product was further purified by vacuum distillation to afford 45.22 g (77.3%) [E, K, E] as a clear, colorless liquid. ¹H NMR (500 MHz, DMSO- d_6) δ 4.16 (s, 4H), 3.46 (q, J = 7.0 Hz, 4H), 1.12 (t, J = 7.0 Hz, 6H).

2.2.2.2 2,5,9,12-tetraoxatridecan-7-one ([ME, K, ME])

To a 1000 mL round bottom flask loaded with 200 mL CH₂Cl₂ at RT was added oxalyl chloride (30 mL, 0.33 mol). The flask was then placed in a dry ice-acetone cooling bath. DMSO

(52 mL, 0.48 mol) mixed with 70 mL CH_2Cl_2 was added slowly over 10 min and maintained for another 10 min until no further gas evolved from the reaction system. Then, addition of [ME, 0, ME] (62.5 g, 0.30 mol) dissolved in 100 mL CH_2Cl_2 occurred over 10 min. The reaction was kept for another 20 min before being quenched by Et_3N (209 mL, 1.50 mol). The cooling bath was removed after 1 h to allow the reaction system to warm to ambient temperature, after which 100 mL deionized water was added. After stirring for 30 min in the presence of water, the mixture was transferred into a 1000 mL separation funnel. Then the upper aqueous layer was collected and the CH_2Cl_2 layer was washed with 3 × 50 mL deionized water. The aqueous layers were combined, washed with 3 × 50 mL Et_2O , followed by removal of water by rotary evaporation under reduced pressure. 300 mL Et_2O was added to the remaining mixture, the precipitate was filtered and Et_2O was removed by rotary evaporation. The remaining product was further purified by vacuum distillation to afford 30.30 g (49.0%) [ME, K, ME] as a clear, colorless liquid. ¹H NMR (500 MHz, DMSO- d_6) δ 4.21 (s, 4H), 3.58 – 3.54 (m, 4H), 3.47 – 3.43 (m, 4H), 3.25 (s, 6H).

2.2.2.3 1,3-bis(2,2,2-trifluoroethoxy)propan-2-one ([F, K, F])

To a 1000 mL round bottom flask loaded with 150 mL CH₂Cl₂ at RT was added oxalyl chloride (20 mL, 0.22 mol). The flask was then placed in a dry ice-acetone cooling bath. DMSO (34 mL, 0.32 mol) mixed with 50 mL CH₂Cl₂ was added slowly over 5 min and maintained for another 10 min until no further gas evolved from the reaction. Then, addition of [F, 0, F] (51.2 g, 0.20 mol) dissolved in 60 mL CH₂Cl₂ occurred over 5 min. The reaction was maintained for another 15 min before quenching with Et₃N (140 mL, 1.0 mol). The cooling bath was removed after 1 h to allow the reaction to warm back to ambient temperature, after which 120 mL deionized water was added. After stirring for 10 min in the presence of water, the mixture was transferred into a

1000 mL separation funnel. Then the bottom CH_2Cl_2 layer was collected and the aqueous layer was washed with 3 × 100 mL CH_2Cl_2 . The organic layers were combined, washed with 3 × 50 mL saturated NaHCO₃ water solution, dried over anhydrous MgSO₄ and filtered, followed by removal of CH_2Cl_2 by rotary evaporation under reduced pressure. The remaining product was further purified by vacuum distillation to afford 40.25 g (79.2%) [F, K, F] as a clear, colorless liquid. ¹H NMR (500 MHz, DMSO- d_6) δ 4.44 (s, 4H), 4.14 (q, J = 9.3 Hz, 4H).

2.2.3 Synthesis of symmetric triethers [R₁, R₂, R₁]

Two symmetric triethers with a glycerol skeleton were obtained from the corresponding 2° alcohol and appropriate halide using the same synthesis strategy while the workup process differed slightly depending on the miscibility of the compounds with water in an effort to maximize the yield.

2.2.3.1 7-(2-methoxyethoxy)-2,5,9,12-tetraoxatridecane ([ME, ME, ME])

To a 250 mL round bottom flask loaded with 100 mL DMSO at RT was added [ME, 0, ME] (62.5 g, 0.30 mol) and NaOH powder (24.7 g, 0.60 mol). The mixture was stirred for 30 min, followed by addition of 2-Chloroethyl methyl ether (CH₃OCH₂CH₂Cl, 57.8 g, 0.60 mol). The temperature was then raised to 50 °C and the reaction stirred at this temperature overnight (~16 h). Upon cooling to RT, the mixture was filtered to remove the solid byproduct. The product was then extracted from DMSO with 3 × 200 mL Et₂O. The ether phase was dried with anhydrous MgSO₄ and filtered, followed by solvent removal by rotary evaporation. The remaining product was further purified by vacuum distillation to afford 42.0 g (52.6%) [ME, ME, ME] as a clear,

colorless liquid. ¹H NMR (500 MHz, DMSO- d_6) δ 3.65 – 3.60 (m, 2H), 3.55 – 3.50 (m, 5H), 3.47 – 3.38 (m, 10H), 3.24 (d, J = 3.5 Hz, 9H).

2.2.3.1 2-(2-methoxyethoxy)-1,3-bis(2,2,2-trifluoroethoxy)propane ([F, ME, F])

To a 250 mL round bottom flask loaded with 100 mL DMSO at RT was added [F, 0, F] (64.0 g, 0.25 mol) and NaOH powder (20.6 g, 0.50 mol). The mixture was stirred for 30 min, followed by addition of 2-Chloroethyl methyl ether (CH₃OCH₂CH₂Cl, 48.2 g, 0.50 mol). The temperature was then raised to 50 °C and the reaction stirred at this temperature overnight (~16 h). Upon cooling to RT, the mixture was filtered first to remove the solid byproduct. The liquid filtrate was poured into 100 mL deionized water. The aqueous phase was then extracted with 3 × 200 mL Et₂O. The organic layers were combined and then washed with 3 × 50 mL deionized water, dried over anhydrous MgSO₄ and filtered. The solvent was removed by rotary evaporation and the remaining was distilled to afford 69.04 g (87.9%) [F, ME, F] as a clear, colorless liquid. 1 H NMR (500 MHz, DMSO- d_6) δ 4.08 (qd, J = 9.4, 1.1 Hz, 4H), 3.72 – 3.59 (m, 7H), 3.46 – 3.41 (m, 2H), 3.25 (s, 3H).

2.3 Property measurements

The ketones and triether products synthesized in this work were stored over 3Å molecular sieves immediate post-distillation to remove trace amount of water. The water content of [ME, ME, ME] and [F, ME, F] were confirmed to be 98.6 and 94.5 ppm, respectively, by a Mettler Toledo C20S Coulometric Karl Fisher titrator using HydranalTM (Coulomat AG) as the reagent. However, data for ketones were not obtained because of the incompatibility of the titration reagent, which contains methanol and can react with ketone to form ketal and water. [11] The dust of molecular

sieves was removed by filtering the liquids through PTFE syringe filters and the liquids were degassed under vacuum for at least 48 h before physical property measurements. Compound densities were measured using a Mettler Toledo DM45 DeltaRange density meter and dynamic viscosity data were obtained from a Brookfield DV-II + Pro viscometer using the same measurement parameters applied in a prior work. ^[12] CO₂ absorption test were conducted following the methods described in our prior works. ^[8] Miscibility of the triether and ketone compounds with common organic solvents and water was determined by mixing 1 mL of a compound with solvent of equal volume thoroughly on a vibrator before standing for 30 min. The liquid pair was determined as 'miscible' when the mixture was homogeneous and clear and would be determined as 'immiscible' if otherwise.

2.4 Calculations

2.4.1 DFT calculations of isolated solvent molecules

Geometry optimizations of the isolated molecules are performed using the B3LYP functional [13, 14] with the 6-31+g(d,p) basis set with dispersion corrections using the DFT-D3 [15] method in Gaussian 09. [16] The single point energy is calculated at a higher level using the M06-2X functional [17] with the Def2-TZVP basis set. Based on the optimized structures of the molecules, the Multiwfn [18-20] program is used to further calculate the general interaction property functions (GIPF) [21] of the studied molecules. These GIPF values are derived from the molecular electrostatic surface potential (ESP) surfaces according to the van der Waals (vdW) surfaces, as defined by Bader [22] (the electron density isosurface corresponding to 0.001 e/Bohr³). The dipole moments of each molecule are calculated from Gaussian during AIMD simulations for

80 femtoseconds (fs) total, with a step size of 0.2 fs. In addition, the COSMO files of the isolated molecules are generated via Gaussian with the BP86 functional [23, 24] at the TZVP level of theory.

The solvent properties(e.g., density, molar volume, and COSMO volume) are calculated at 25 °C, along with the σ -surfaces and σ -profiles, using COSMOThermX based on the COSMO-RS approach. [25, 26] The fractional free volume (FFV) is an important parameter to describe the free volume effect for gas solubility in many different materials, including the CO₂ solubility in multivalent ionic liquids (ILs). [27, 28] Shannon, et~al. proposed that for some ILs, the FFV can be estimated using a COSMO approach as: $FFV_{\rm cosmo} = (V_{\rm m} - V_{\rm cosmo})/V_{\rm m}$. [29] Likewise, this approach is used here to estimate the FFVs of the studied organic molecules.

2.4.2 DFT calculations of CO₂ adsorption to solvent molecules and among solvent dimers

To further investigate the competitive interactions in the solvents, we calculate the adsorption of CO₂ to the isolated solvent molecules, as well as the interaction between solvent molecule dimer models. The structural optimization and screening strategy are described below.

First, more than 1,000 structures are generated using the Molclus ^[30] program and serve as initial the structures for semi-empirical quantum mechanical optimization using CREAST ^[31] with GFN0-xTB ^[32, 33] and xTB version 6.3.2. Second, the obtained isomers are then used as candidate structures and further optimized with GFN2-xTB. ^[34] Then, the fie lowest-energy isomers obtained are calculated at the B97-3c ^[35] level using ORCA 4.2.0. ^[36, 37] Furthermore, geometric optimizations of the three lowest-energy structures are further performed using B3LYP-D3/6-31+g(d,p) in Gaussian 09, along with frequency calculations to obtain the zero-point

vibrational energies (ZPEs). Finally, the binding energies of the solvent molecules with CO₂ and between the solvent dimer models are calculated from the single point energy structures at a higher level with M06-2X/Def2-TZVP. Counterpoise (CP) corrections are also applied in order to account for basis set superposition errors (BSSE). [38]

The interaction energy ($E_{\rm int}$) is defined in Eqn. 1 as the total energy of the relaxed complex ($E_{\rm complex}$) minus the sum of the energies of the isolated solvent molecule and the CO₂ molecule or the second solvent molecule ($E_{\rm CO_2}^*$ and $E_{\rm mole}^*$, respectively) corresponding to the geometries of these species obtained from the bound complex (indicated with an asterisk).

$$E_{\text{int}} = E_{\text{complex}} - (E_{\text{mole}}^* + E_{\text{CO}_2}^*) \text{ or } E_{\text{int}} = E_{\text{complex}} - 2 \cdot E_{\text{mole}}^*$$
 (1)

In comparison, the binding energy $(E_{\rm bind})$ is defined as the energy difference between the relaxed complex and the relaxed separated species in their lowest energy geometries. Furthermore, these energy values can be subdivided into the interaction energy $(E_{\rm int})$ between the molecules in the complex, the zero-point vibrational energy difference $(\Delta E_{\rm ZPE})$, and the deformation energy $(E_{\rm def})$ as shown in Eqn. 2. The last term accounts for the energy involved with the structural changes of the molecules in order to adopt the new geometry found in the relaxed complex. [39]

$$E_{\rm bind} = E_{\rm int} + \Delta E_{\rm ZPE} + E_{\rm def} \tag{2}$$

In order to further investigate the structure-property relationships of these studied molecules, as well as the intermolecular interactions with CO_2 or solvent dimers, the electrostatic surface potential (ESP), the reduced density gradient (RDG) [40], and the independent gradient model [41] (IGM) are analyzed by Multiwfn and visualized using VMD. [42]

3. Results and Discussion

3.1 Screening of synthesis strategies

Three symmetric 2° alcohol compounds in the form of [R₁, 0, R₁] were synthesized at molar scales from epichlorohydrin and a corresponding primary (1°) alcohol by adopting different strategies to maximize purity and yield. EtOH was used first to get [E, O, E] as a benchmark reaction. As the use of Na⁰ leads to a clean reaction with little impurities as noted in our previous work, [9] water was not used to wash the organic phase in order to diminish the loss of organic compound despite of the immiscibility of [E, 0, E] with water. As a result, the yield increased from 55.8% to 73.8%. However, in the synthesis of [ME, 0, ME], the product is not only soluble in water, but has a partition coefficient $(P = C_0/C_W) < 1$ when using CH_2CI_2 or Et_2O as the extractant. In this case, Et₂O was used just for dilution and salt precipitation purposes and the product was directly distilled from the water phase. Here an increase in yield from 40.2% to 63.0% was observed, although it is still relatively low when compared with [E, O, E] and [F, O, F] which prefer organic solvent. To avoid the operational complexity of using Na⁰ and reduce the amount of 1° alcohol needed, [F, O, F] was synthesized in aq. NaOH using trifluoroethanol at 2.2 eq. relative to epichlorohydrin due to the strong electronegativity of fluorine atoms which makes it easier to activate the alcohol as a nucleophile to initiate the reaction. Moreover, the trifluoroethyl functional group also helps reduce water solubility compared to ethyl or methoxyethyl groups, as [F, O, F] separates from water after reaction. Unfortunately, the efficiency of water phase reaction is highly limited by the nature of the primary alcohol used, as we noticed that the yield of [F, O, F] reached 75.7% while the yield for [E, O, E] and [ME, O, ME] using the same reaction

conditions were just 22.7% and 13.6%, respectively, with the majority of product as oligomers and monoethers of glycerol.

Apart from the 2° alcohol, [R₁, 0, R₁], the hydrophilicity/hydrophobicity of functional groups also affected the synthesis procedure and efficiency of the Swern oxidation used to form the ketones. Similar post-reaction process strategies as [R₁, 0, R₁] were adopted, and the yields of [E, K, E], [ME, K, ME] and [F, K, F] were 77.3%, 49.0% and 79.2%, respectively, which are approximately the same as for the 2° alcohols, [R₁, 0, R₁]. This correlates to the hydrophilicity of the functional groups in the sequence of CH₃OCH₂CH₂- > CH₃CH₂- > CF₃CH₂-. This was confirmed in the synthesis of [ME, ME, ME] and [F, ME, F] where [ME, ME, ME] readily dissolved in water, while [F, ME, F] was purified from the organic phase. It is also worth mentioning that the NaOH/DMSO system is highly effective in the nucleophilic substitution between 2° alcohol and halide. This catalyst/solvent combination might be utilized for complete alkylation of glycerol at ambient temperature to obtain more symmetric 1,2,3-triether (i.e., [R₁, R₁, R₁]) compounds and we are exploring this approach. The overall yields of [E, K, E], [ME, K, ME], [F, K, F], [ME, ME, ME] and [F, ME, F] were 57.0%, 30.9%, 60.0%, 33.1% and 66.5%, respectively.

3.2 Density

Densities of ketones and triethers developed in this work were measured at 1 atm over a temperature range from 293.15 to 353.15 K with 10 K increments. The results are plotted in Figure 1 with a detailed data table provided in Table S1. A linear regression equation was obtained for each compound and the corresponding parameters are shown in Table 2. The linearity of these fits are confirmed by $R^2 = 1.000$ with a maximum deviation of < 0.02%, making

it reasonable to predict compound densities over this range. As a result, the densities of solvent studied at 303.15 K, 318.15 K, 333.15 K and 348.15 K were calculated from the regression equations and used in the CO₂ absorption calculations.

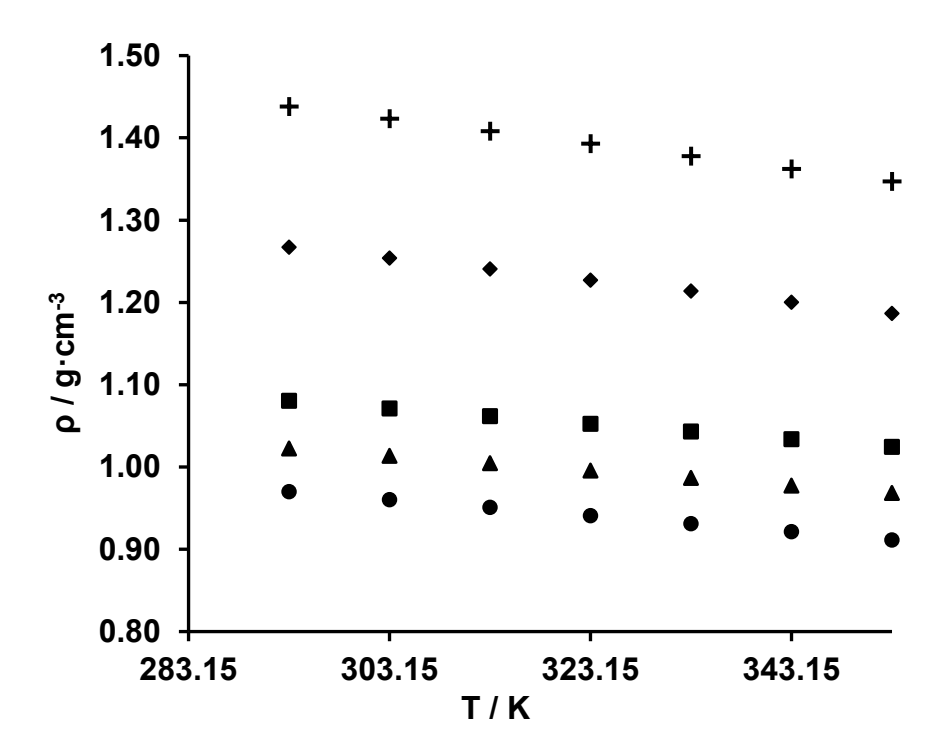


Figure 1: Relationship between the density and temperature for ketones and triethers studied in this work. Circle = [E, K, E]; square = [ME, K, ME]; cross = [F, K, F]; triangle = [ME, ME, ME]; diamond = [F, ME, F].

Table 2: Parameters of the density-temperature linear fit ($\rho = -a \cdot T + b$) for compounds studied in this work within a temperature range of 293.15 – 353.15 K.

Compound	$\frac{a}{10^{-4} \cdot \mathbf{g} \cdot \mathbf{cm}^{-3} \cdot \mathbf{K}}$	$\frac{b}{\mathbf{g} \cdot \mathbf{cm}^{-3}}$	R ²	Maximum Deviation (%)	
[E, K, E]	9.792	1.257	1.0000	0.016	
[ME, K, ME]	9.367	1.355	1.0000	0.005	
[F, K, F]	15.209	1.884	1.0000	0.017	
[ME, ME, ME]	8.989	1.286	1.0000	0.004	
[F, ME, F]	13.402	1.660	1.0000	0.018	

In general, the density for symmetric compounds based on glycerol skeleton with the same functional group modification at specific temperatures follows the trend: $[R_1, K, R_1] > [R_1, 0, R_1] > [R_1, R_1, R_1]$, which can be confirmed by compounds with CH_3CH_2 - and $CH_3OCH_2CH_2$ - group. This rule also applies to comparison between [F, 0, F] and [F, K, F]. Data absent for $[R_1, 0, R_1]$ and [E, E, E] can be found in our previous work. $^{[9, 10]}$ Given that the molecular weights of the three kind of compounds is in the reverse order, the molar volume (V_m) is in the order of $[R_1, R_1, R_1] > [R_1, 0, R_1] > [R_1, K, R_1]$. It is worth mentioning that the DFT calculated volume, \tilde{V}_m (ų), obtained in Table S9 at 293.15 K are compared with the measured values in Table 3, and the predicted data are found to be close to measured values with absolute percent deviation for [E, K, E], [ME, K, ME], [F, K, F], [ME, ME, ME] and [F, ME, F] being 2.0%, 0.0%, 2.2%, 1.6% and 3.3%, respectively, indicating the suitability of simulation model.

Table 3: Measured and DFT predicted molar volume at T = 293.15 K and p = 101 kPa.^a

	Molar volume (cm³·mol⁻¹)								
	[E, K, E]	[ME, K, ME]	[F, K, F]	[ME, ME, ME]	[F, ME, F]				
V _m	150.68	190.84	176.70	260.46	247.98				
V _{m_cal}	147.67	190.89	172.84	256.27	239.87				

^a Uncertainty: $u(V) = 0.01 \text{ cm}^3 \cdot \text{mol}^{-1}$.

3.3 Viscosity

The dynamic viscosity of the compounds developed in this work were measured at 1 atm and at T = 293.15, 298.15, 303.15, 308.15, 313.15, 318.15, 323.15, 333.15, 343.15 and 353.15 K, and these are shown in Figure 2 with detailed data provided in Table S2. Moreover, viscosity data

were fitted to the Andrade Equation in the form of η = a · exp(b/T) with good agreement. Fit parameters are shown in Table 4.

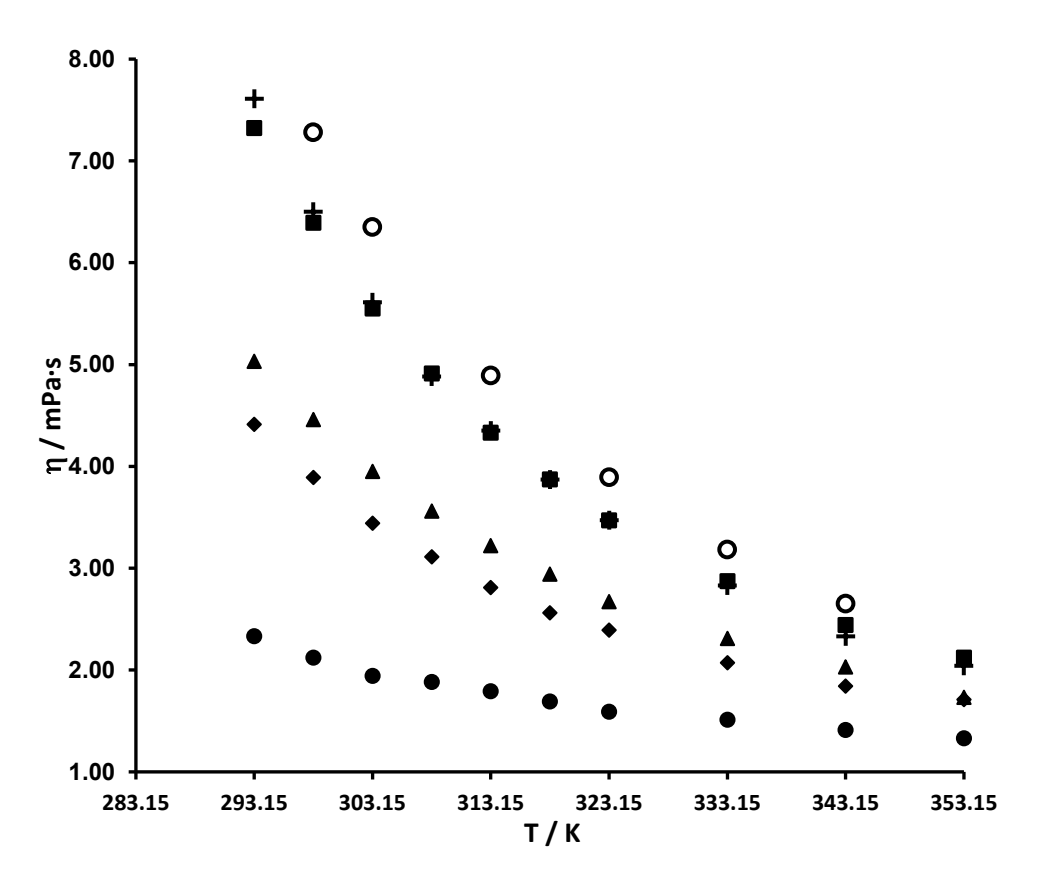


Figure 2: Relationship between viscosity and temperature for ketones, triethers and DMPEG. Circle = [E, K, E]; square = [ME, K, ME]; cross = [F, K, F]; triangle = [ME, ME, ME]; diamond = [F, ME, F]; hollow circle = DMPEG.

Table 4: Viscosity-temperature equation ($\eta = a \cdot \exp(b/T)$) parameters for symmetric compounds over the range of T = 293.15 – 353.15 K.

Compound	$\frac{a}{mPa \cdot s}$	b K	R ²
[E, K, E]	9.2339 x 10 ⁻²	0.931×10^3	0.9778
[ME, K, ME]	0.4505 x 10 ⁻²	2.158×10^3	0.9960
[F, K, F]	0.3047 x 10 ⁻²	2.281×10^3	0.9962
[ME, ME, ME]	1.0060 x 10 ⁻²	1.812×10^3	0.9964
[F, ME, F]	1.4955 x 10 ⁻²	1.650×10^3	0.9850

Considering the viscosities of 2° alcohols ^[9], ketones and triethers, it is clear that the solvent viscosity follows $[R_1, 0, R_1] > [R_1, K, R_1] > [R_1, R_1, R_1]$, which relates to the presence/absence of H-bonding and intermolecular forces when alcohol is transformed to a ketone, while the molecular interactions are further depressed as a result of alcohol elimination and branch extension due to formation of a less polar ether group in triethers.

Viscosity is an important factor in evaluation of a solvent candidate for applications, as it correlates to pressure drop, and mass/heat transfer rates. Although there is usually a trade-off between solvent volatility and viscosity, less viscous liquids are preferred in many applications including continuous absorption-stripping processes. To validate the potential of solvents developed for CO₂ removal in terms of viscosity, data for DMPEG from Li, et al. [43] are included in Figure 2. It shows that all five glycerol derivatives have lower viscosities than DMPEG (as well as solvents such as ILs), which means less energy costs for liquid transport and may provide advantages for device simplification. From this perspective, the compounds developed are suitable substitutes of DMPEG for CO₂ absorption.

3.4 CO₂ solubility

The CO₂ capacity of the compounds developed was determined at T = 303.15, 318.15, 333.15 and 348.15 K in the range of P = 2 - 10 atm. Solubility data are provided in Table S3-S7. Table 5 shows the slope (m) obtained from the linear regression equation of x-P (Figures S6-S10), deviation parameters (average absolute percent deviation, AAPD [10]), R² value, Henry's constants, volumetric concentration (S_v) and molality (S_m). Given that the intercept of the linear regression was forced through the origin, the small deviation and R² value approaching or equaling 1

indicates excellent agreement of solvent behavior with Henry's law and confirms the physical (i.e., non-reactive) nature of the solvent in a CO₂ capture process.

Table 5: CO₂ solubility parameters of compounds studied at relevant temperatures.^{a,b}

Compound	$\frac{T}{K}$	$\frac{m}{10^{-2} \cdot atm^{-1}}$	AAPD (%)	R²	$\frac{H_{CO_2}}{atm}$	S _v (cm³(STP)c m ⁻³ atm ⁻¹)	S _m (mol kg ⁻¹ atm ⁻¹)
	303.15	1.966	1.502	0.9998	50.9 ± 0.8	3.17 ± 0.08	0.147 ± 0.004
[ר ע ר]	318.15	1.569	1.678	0.9998	63.7 ± 1.1	2.48 ± 0.05	0.117 ± 0.002
[E, K, E]	333.15	1.283	1.205	0.9999	78.0 ± 0.9	1.98 ± 0.05	0.095 ± 0.002
	348.15	1.077	0.802	0.9999	92.8 ± 0.7	1.62 ± 0.04	0.079 ± 0.002
	303.15	2.054	2.028	0.9998	48.7 ± 1.0	2.65 ± 0.04	0.110 ± 0.002
[NAE 1/ NAE]	318.15	1.620	1.475	0.9999	61.7 ± 0.9	2.04 ± 0.04	0.086 ± 0.002
[ME, K, ME]	333.15	1.313	1.214	0.9999	76.2 ± 0.9	1.61 ± 0.03	0.069 ± 0.001
	348.15	1.096	0.679	1.0000	91.2 ± 0.6	1.32 ± 0.03	0.057 ± 0.001
	303.15	2.218	0.688	1.0000	45.1 ± 0.3	3.08 ± 0.12	0.096 ± 0.004
[ב ע ב]	318.15	1.762	0.144	1.0000	56.8 ± 0.1	2.38 ± 0.10	0.076 ± 0.003
[F, K, F]	333.15	1.448	0.341	1.0000	69.1 ± 0.2	1.91 ± 0.07	0.062 ± 0.002
	348.15	1.221	0.237	1.0000	81.9 ± 0.2	1.58 ± 0.05	0.052 ± 0.002
	303.15	2.944	1.162	0.9999	34.0 ± 0.4	2.86 ± 0.20	0.126 ± 0.009
[318.15	2.307	1.216	0.9999	43.3 ± 0.5	2.18 ± 0.15	0.097 ± 0.007
[ME, ME, ME]	333.15	1.874	0.970	0.9999	53.4 ± 0.5	1.74 ± 0.11	0.079 ± 0.005
	348.15	1.557	1.072	0.9999	64.2 ± 0.7	1.41 ± 0.09	0.065 ± 0.004
	303.15	3.166	4.398	0.9988	31.6 ± 1.4	3.35 ± 0.05	0.119 ± 0.002
[E N/E E]	318.15	2.555	3.960	0.9991	39.1 ± 1.5	2.63 ± 0.04	0.095 ± 0.002
[F, ME, F]	333.15	2.105	3.910	0.9991	47.5 ± 1.9	2.12 ± 0.03	0.078 ± 0.001
	348.15	1.775	4.135	0.9990	56.4 ± 2.3	1.75 ± 0.02	0.065 ± 0.001

^a Uncertainties are u(T) = 0.01 K, u(m) = 0.001, u(AAPD) = 0.001 and $u(R^2) = 0.0001$.

The H_{CO_2} values in Table 5 indicate CO_2 affinity of compounds are in the order of [F, ME, F] > [ME, ME, ME] > [F, K, F] > [ME, K, ME] > [E, K, E]. It is also found that both triethers and ketones exhibit higher CO_2 capacity over corresponding 2° alcohols when comparing to data from our previous work. [9] It is plausible that the elimination of the -OH groups when converting [R₁, 0, R₁] into ketones and triethers contributes to increased CO_2 affinity as a consequence of H-bond

^b m is the inverse of the Henry's Constant (i.e., $m = 1/H_{CO_2}$).

reduction, which leads to less interactions between solvent molecules and more interactions with CO₂. Similar phenomena have been observed by Henni et al. ^[44] and Amaral et al. ^[45] in the alkylation of polyethylene glycol (PEG) where alkylated oligomer components exhibited higher CO₂ capacity compared to unmodified PEG with two -OH groups at the end of the backbone. The superior performance of triethers over ketones may be contributed to an increase in free volume, which can be calculated using computed molar volume and COSMO volume data in Table S9 by Eqn 3:

$$V_{F_cal}$$
 (cm³·mol⁻¹) = (\tilde{V}_m - V_{COSMO}) (Å³/molecule) × (10⁻²⁴ cm³/Å³) × (6.02 × 10²³ molecules/mol) (3)

The calculated molar free volume, V_{F_cal} , for [E, K, E], [ME, K, ME], [F, K, F], [ME, ME, ME] and [F, ME, F] are 30.80, 33.13, 26.16, 47.28 and 42.25 cm³·mol⁻¹, respectively. V_{F_cal} increased 42.7% from [ME, K, ME] to [ME, ME, ME] and 61.5% from [F, K, F] to [F, ME, F] as a result of chain extension on C2, which creates higher barriers for solvent molecule interaction than for the corresponding carbonyl group. However, the molar free volume is not the sole factor for the change in CO₂ capacity, as the order of V_{F_cal} for the five compounds studied does not strictly follow CO₂ affinity order. Apart from molar free volume, the chemical characteristic of the function groups is assumed to be another dominant factor in the solvent behavior. From this perspective, the ether group and the fluorine atoms, combined with evidence from our previous study, ^[9] have proved to be highly efficient in CO₂ capture, while the field of glycerol modification with other functional groups remains open for improvement.

Apart from CO_2 capacity, H_{CO_2} is also helpful for revealing thermal features of absorption using the van't Hoff equation (Eqn. 4):

$$\frac{d(\ln H_{CO2})}{d(\frac{1}{T})} = -\frac{\Delta H_{abs}}{R} \tag{4}$$

Where T (K) is temperature, ΔH_{abs} (kJ·mol⁻¹) is the enthalpy of absorption, and R (kJ·K⁻¹·mol⁻¹) is the gas constant. To understand temperature dependance of Henry's constant, H_{CO_2} , more intuitively, Eqn. 4 can be integrated into the form of Eqn. 5:

$$\ln H_{CO_2} = -\frac{\Delta H_{abs}}{R} \cdot \frac{1}{T} + b \tag{5}$$

and fit parameters are shown in Table 6 with correlation coefficients greater than 0.999 and maximum deviation less than 0.7% for all compounds studied. The enthalpies of absorption are calculated to be -11.7, -12.3, -11.6, -12.4 and -11.3 kJ·mol⁻¹ for [E, K, E], [ME, K, ME], [F, K, F], [ME, ME, ME] and [F, ME, F], respectively. As expected, ΔH_{abs} does not vary too much for glycerol derivatives ([R_1 , 0, R_1] [9], [R_1 , K, R_1] and [R_1 , R_1 , R_1]) and ILs [46] in the literature, with values between -9 and -15 kJ·mol⁻¹. Apart from ΔH_{abs} , parameters in Table 6 were used for predicting H_{CO_2} over a reasonably expanded temperature range from 273.15 K to 353.15 K to allow comparison of solvent behavior with that of DMPEG series compounds, as well as selected IL physical solvents. In this study, the H_{CO_2} value for DMPEG [CH₃O(CH₂CH₂O)_nCH₃] and certain PEG ethers (Glyme, n = 1; Diglyme, n = 2; Triglyme n = 3 and Tetraglyme, n = 4) are extrapolated from work done by Henni et al. [44] Moreover, 1-butyl-3-methylimidazolium hexafluorophosphate ([C₄mim][PF₆]) [47] was selected as it is a recognized IL with high CO₂ performance, and 1-n-hexyl-3-methylimidazolium bis(trifluoromethylsulfonyl)imide ([C6mim][Tf2N]) was also considered for its high performance in CO_2 removal [46]. The H_{CO_2} temperature dependence of all compounds studied is shown in Figure 3. It is clear that [ME, ME, ME] and [F, ME, F] are superior in terms of CO₂ affinity over the other compounds, with one exception for Tetraglyme (298.15 K, 29.6 atm). It is also noted that DMPEG oligomers have higher CO₂ affinity as repeat unit (n) increases and may surpass [ME, ME, ME] and [F, ME, F] at 298.15 K when n is equal or larger than 5. However, the complexity of synthesizing monodisperse PEG with exact repeat units hindered the application, and thus compromise between cost and performance resulted in the utilization of DMPEG, the mixture of oligomers, which is less effective than [ME, ME, ME] and [F, ME, F].

Apart from DMPEG, the two triethers also are superior to these ILs. It is worth mentioning that although some task-specific ILs can achieve equal-molar [48] or even multi-molar [49] equivalents of CO₂ absorption at ambient temperature and pressure as chemical solvents through activation of functional groups, the solvent regeneration process makes it less attractive as reaction between ILs and CO₂ requires large energy inputs. From this perspective, traditional ILs might be a better choice for comparing the enthalpy of absorption given that the enthalpy of desorption is also at the same level as glycerol derivatives and DMPEG. Figure 3 also shows that the H_{CO_2} - T curve tends to bend upward upon increasing temperature, meaning that solvents lose CO₂ affinity more rapidly at higher temperature. This phenomenon applies to all solvents in Figure 3 while, in general, the H_{CO_2} of [ME, ME, ME] and [F, ME, F] are less sensitive to temperature than DMPEG and ILs, which provides more flexibility for operation and process intensification when used in an absorption process. Unlike H_{CO_2} , other performance metrics, volumetric concentration (S_v) and molality (S_m) , do not necessarily correlate with the change of Henry's constant, as more variables such as density and molecular weight are involved in determination of corresponding parameters. For example, [ME, K, ME] is superior to [F, K, F] but yield when compared to the S_m value of [ME, ME], while the difference in molecular weight and CO_2 affinity lead to the least CO_2 capacity when considering H_{CO_2} value.

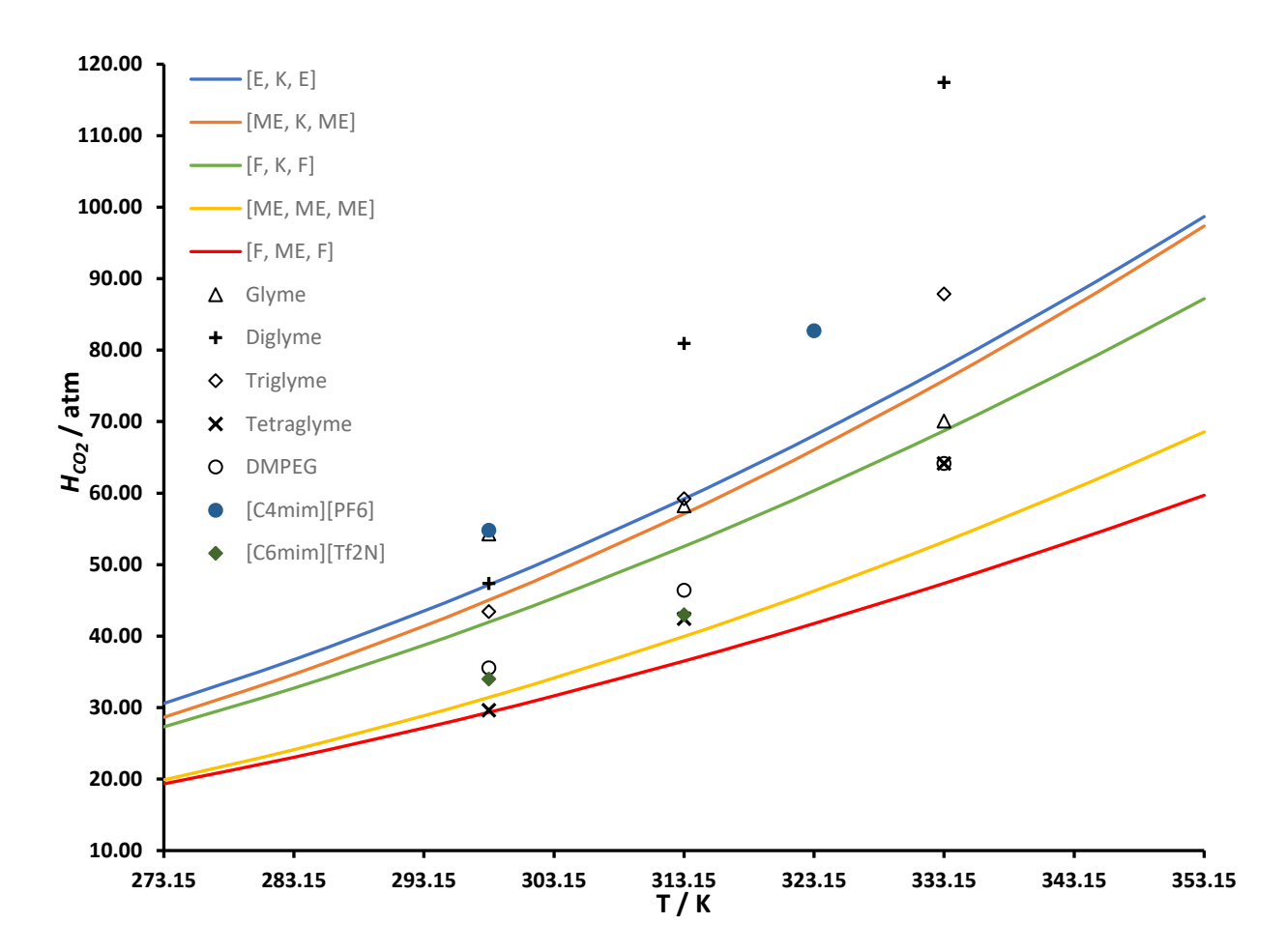


Figure 3: Temperature dependence of H_{CO_2} for the ketones and triethers developed in this work, a DMPEG series of compounds, and chosen ILs.

Table 6: Henry's constant-Temperature fit parameters of compounds studied.

		$\ln H_{CO_2} = -\frac{1}{2}$	$\frac{\Delta H_{abs}}{2} \cdot \frac{1}{2} + b$	
Compounds	$\frac{\Delta H_{abs}}{R}$ / K	b	$\frac{R}{R^2}$	Maximum Deviation (%)
[E, K, E]	1412.7	8.5922	0.9998	0.45
[ME, K, ME]	1475.2	8.7557	0.9996	0.52
[F, K, F]	1399.9	8.4322	0.9993	0.68
[ME, ME, ME]	1492.8	8.4549	0.9995	0.65
[F, ME, F]	1359.5	7.9390	0.9999	0.26

3.5 Calculation results

3.5.1 DFT results for isolated solvent molecules

The DFT-optimized structures of the isolated solvent molecules are shown in Figure S11, the corresponding σ-surfaces are shown in Figure S12, and the electrostatic potential (ESP) surfaces are shown in Figure 4. The minimum ESP regions of the molecules are shown in blue, which tend to correspond to the red areas shown in the σ -surfaces, indicating electron-dense regions. While the maximum ESP regions of the molecules are shown in red, which tend to correspond to the blue areas shown in the σ-surfaces, indicating electron-sparse regions. The local minima (blue spheres) of the blue ESP regions or local maxima (red spheres) of the red ESP regions are the most likely binding site with positively/negatively charged atoms, e.g., C of CO₂, or O of CO₂, respectively. With respect to these solvents, the -CH₂ groups contribute to the positive ESP, the O atoms contribute to the negative ESP, while the -CF₃ groups are controlled by the neighbors. A comparison of the σ-profile with the ESP distribution of the studied molecules is shown in Figure S13. The GIPF descriptors of the studied molecules are listed in Table S8. Among these parameters, the molecular polarity index (MPI)30⁵⁰ is used to describe the polar nature of neutral molecules. Here, the order of polarity of these studied solvent molecules is found to be: [F, K, F] > [F, ME, F] > [E, K, E] > [ME, K, ME] > [ME, ME, ME]. The weak intramolecular vdW interactions can be seen from the reduced density gradient (RDG) maps in Figure S14; these interactions stabilize the lowest energy conformers.

Min Max

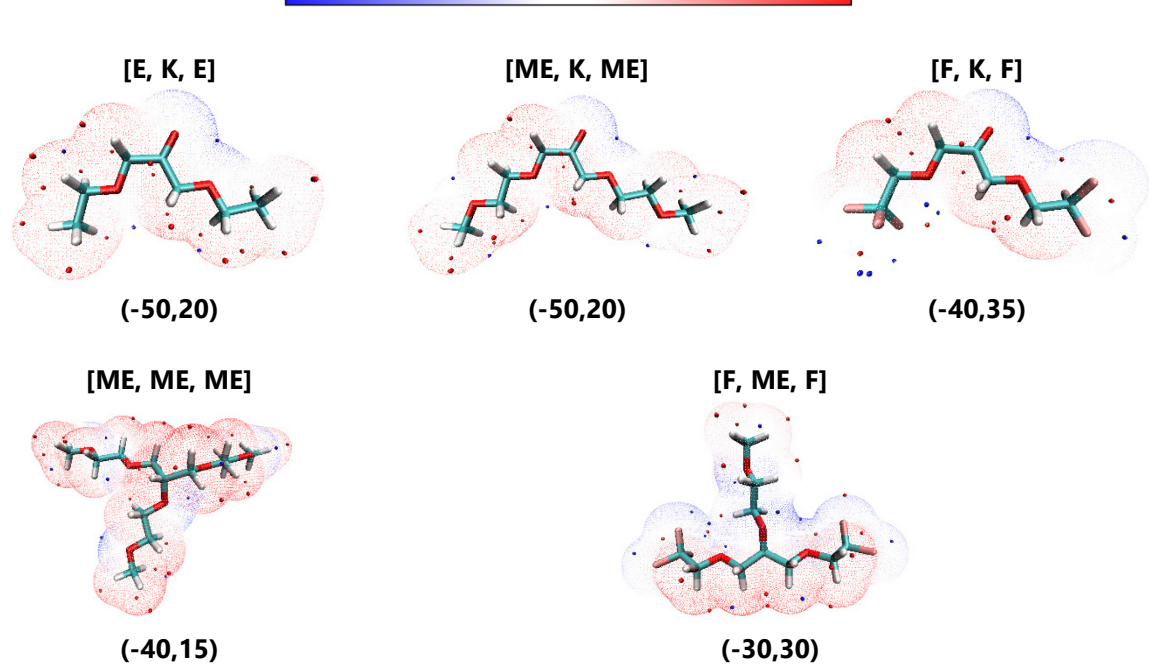


Figure 4. Electrostatic potential surfaces of the studied molecules, corresponding to the ρ = 0.001 e/Bohr³ isosurface. The color scale bar is shown at the top, while the corresponding ESP values (units of kcal/mol) are shown in parentheses. The blue and red spheres on the ESP surface are local minima and maxima points, respectively. These molecules are represented as licorice models (cyan: C, white: H, red: O, blue: N, and pink: F).

The DFT calculated dipole moments of isolated molecules in the gas-phase are listed in Table S9. The dipole moments during the AIMD simulations are shown in Figure S15, indicating that the dipole moment is sensitive to the configurations, which could compromise its reliability for describing the polarity of molecules. The predicted solvent properties using COSMO-RS are listed in Table S9. The [E, K, E] solvent shows the highest FFV (0.209), while the [F, K, F] solvent shows the lowest FFV (0.151).

3.5.2 DFT results for CO₂ adsorption to solvent

The most stable structures of CO₂ adsorbed to the studied solvent molecules are shown in Figure S16. With regard to the previously mentioned ESP surfaces of these single molecules

(Figure 4), we can see that the CO₂ species are most likely to bind with the blue regions of the solvents. Besides, the IGM maps (Figure 5) illustrate the vdW interactions between CO₂ with the solvents. The C atom of CO₂ is responsible for the highest contribution to the overall intermolecular interactions, while the O atom of the solvent molecules surrounding the blue ESP regions provide the greatest contribution from the solvents. Furthermore, the ESP of the vdW surfaces (Figure 6) between these solvents interacting with CO₂ show that the nature of these non-covalent interactions are strongly dictated by the overlapping regions of opposing ESP values, which is indicative of electrostatic complementarity.

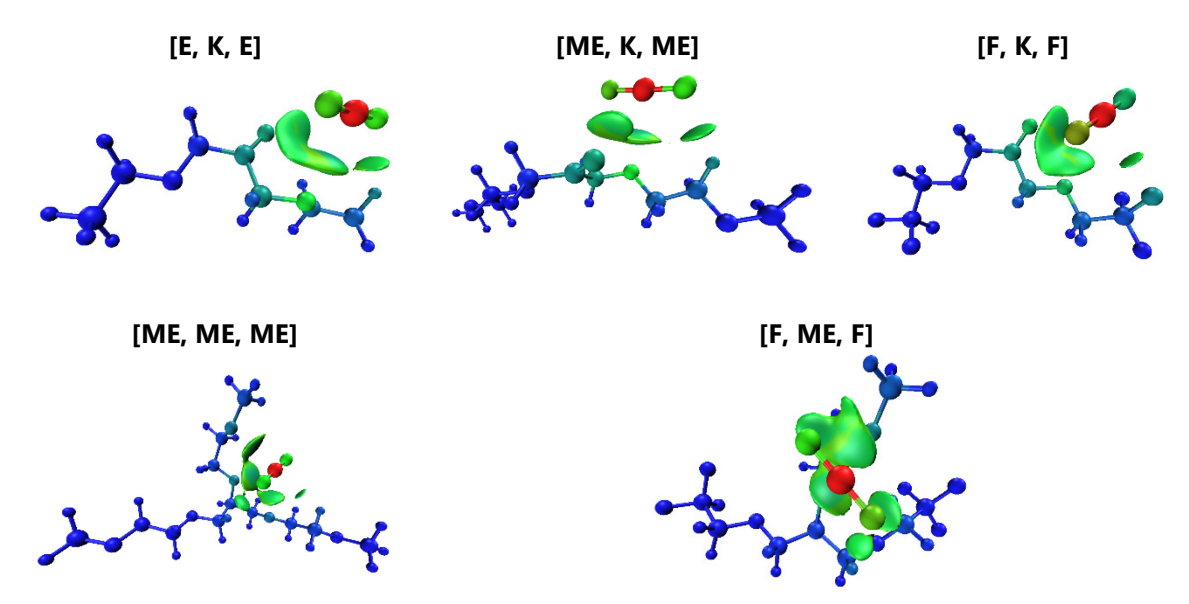


Figure 5. IGM maps of the most likely sites for CO_2 interaction with the studied solvent molecules. The isovalue of the IGM is set to 0.5 au. The surfaces/atoms are colored on a blue-green-red scale. Blue indicates strong attractive interactions/low contribution to the intermolecular interaction, and red indicates strong nonbonded overlap/high contribution to the intermolecular interaction.

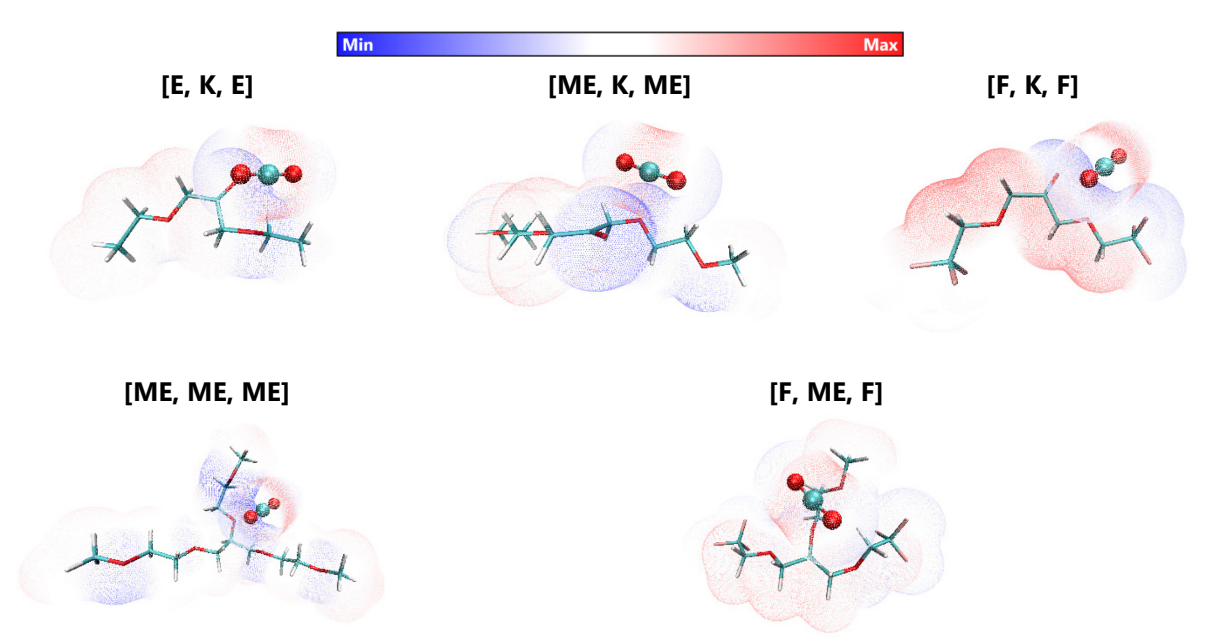


Figure 6. ESP overlap analysis of the vdW surfaces of the most stable adsorbed sites for CO₂ interacting with the studied solvent molecules. Each fragment in the system is colored corresponding to (-50, 50) kcal/mol.

3.5.3 DFT results for solvent-solvent interaction

The most stable structures of the solvent dimers are shown in Figure S17. Because the solvent molecules are large, the adsorption interactions between the solvent molecule are much more complex than with CO₂. The IGM maps of the dimers (Figure 7) show that the intermolecular interactions are dominated by the vdW interactions, but small pieces of H-bonding are found between O atoms with H-C. Besides, the ESP overlap of the dimer vdW surfaces (Figure 8) also show that there is electrostatic complementarity between the solvent pairs.

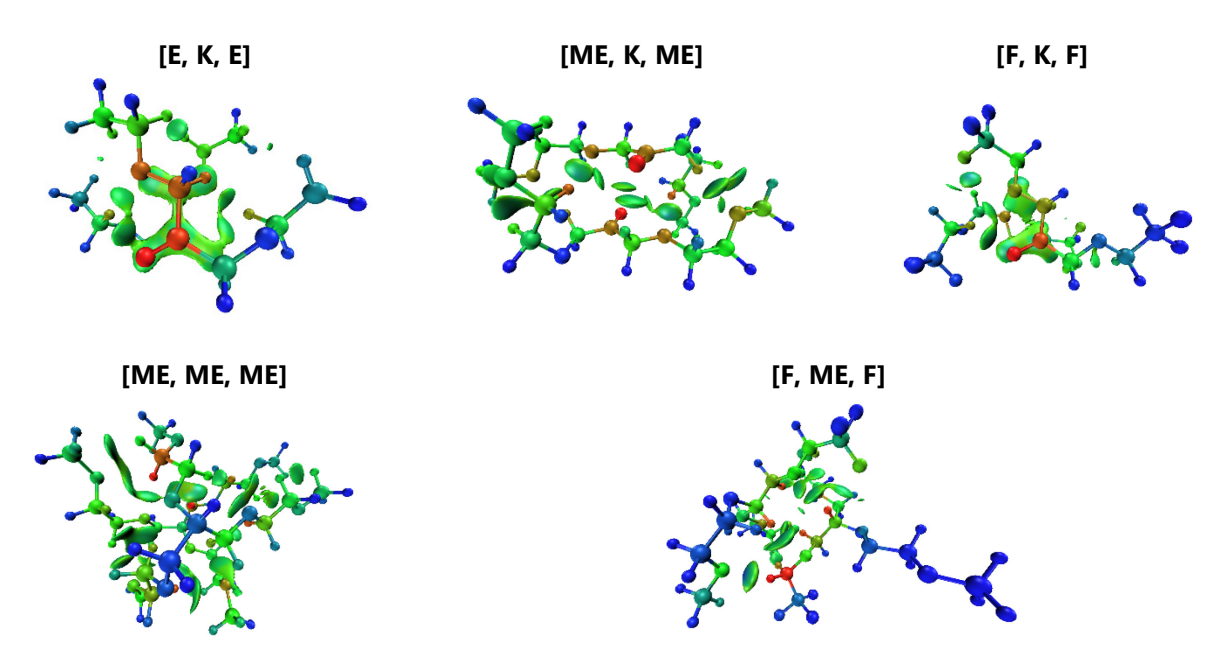


Figure 7. IGM maps of the most stable structures of the solvent dimers. The same color code is used as in Figure 5.

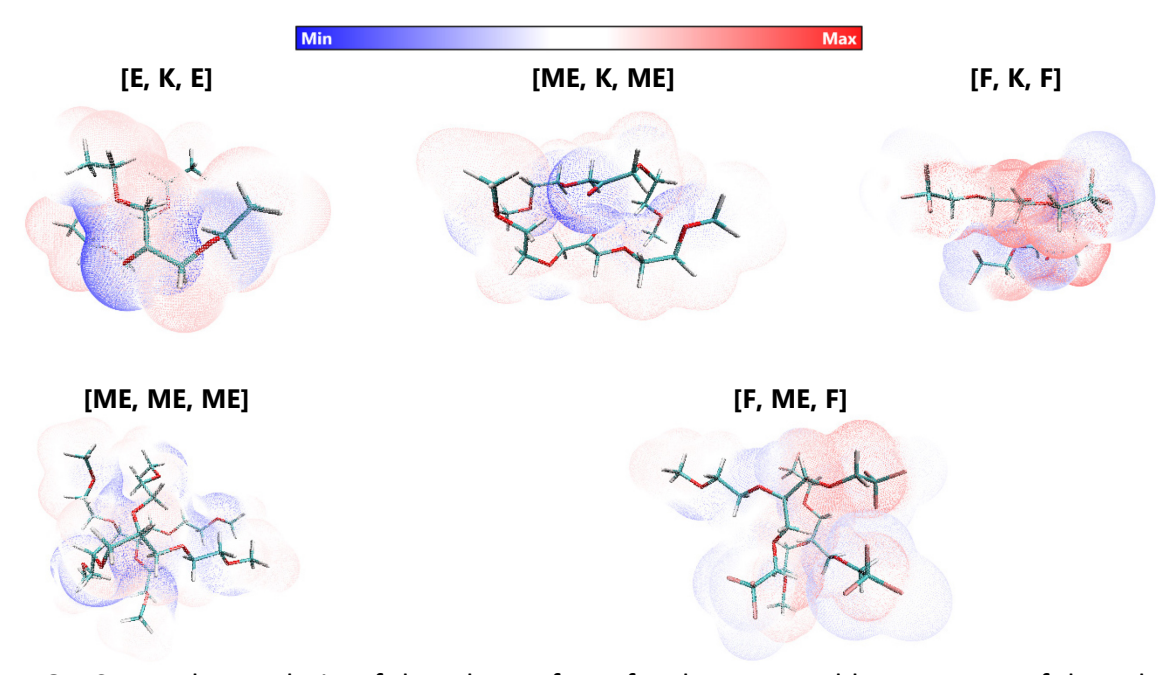


Figure 8. ESP overlap analysis of the vdW surfaces for the most stable structures of the solvent dimers. The same color code is used as in Figure 6.

3.5.4 Competitive adsorption between CO₂ versus neighboring solvent molecules

As discussed previously, the intermolecular interactions between the solvents with CO₂ or with neighboring solvents are strongly influenced by electrostatic complementarity. Thus, if a solvent molecule adsorbs a CO₂ molecule, the CO₂ molecule has to compete with neighboring solvent molecules (although, due to significant size differences, the neighboring solvent would not be completely displaced). The comparison of binding energy between solvent-CO2 with solvent-solvent is calculated and listed in Table 7. As established previously, the free volume and the affinity of CO₂ to the solvent are two primary factors controlling the CO₂ solubility in ILs. [27] Here, we use the binding energy between CO₂ with the solvent to quantify the CO₂ affinity. While the binding energy between the solvent dimers is used to quantify the binding strength among neighboring solvents. Theoretically, a stronger binding energy between solvents indicates a smaller FFV, which is confirmed by the calculated FFV_{cosmo} . Thus, the key to improve the solubility of CO₂ in these organic solvents should be to increase the affinity of CO₂ to the solvents while simultaneously decreasing the interaction between the solvents. However, due to the complex molecular interactions in these systems, no single parameter has emerged as a definitive indication of CO₂ adsorption performance. Regardless, the DFT calculation provide much more molecular-level insight that can help clarify the balance between the solvent-solute and solventsolvent interactions.

Table 7. Interaction energy and binding energy (units of kcal/mol) between the studied molecules and CO_2 in vacuum, as well as the interactions within solvent dimers.

SolventCO ₂				Solvent	.Solvent			
	$E_{ m int}$	ΔE_{ZPE}	$E_{ m def}$	$E_{ m bind}$	$E_{ m int}$	ΔE_{ZPE}	$E_{ m def}$	$E_{\rm bind}$
[E, K, E]	-6.26	0.97	-1.04	-6.32	-14.66	1.95	2.81	-9.90
[ME, K, ME]	-5.99	0.95	-0.97	-6.00	-24.57	3.17	7.00	-14.39
[F, K, F]	-5.47	0.68	0.26	-4.53	-18.60	2.19	0.78	-15.63
[ME, ME, ME]	-8.90	1.04	1.19	-6.68	-19.73	3.36	3.77	-12.59
[F, ME, F]	-6.49	1.39	-2.68	-7.78	-13.55	1.96	-1.77	-13.36

3.6 Miscibility evaluation

Given that ketones and triethers based on glycerol skeletons developed in this work have been shown to have low viscosity and good performance for CO₂ capture, it is important to understand the miscibility of these compounds with common solvents to expand applications such as synthesis and solvation process. Table 8 shows the miscibility of [E, K, E], [ME, K, ME], [F, K, F], [ME, ME] and [F, ME, F] with common organic solvents ranging from hexanes (least polar) to DMSO (most polar) in the order of increased polarity based on the dipole moment values. Apart from hexane and water, the ketones and triethers were generally consistent and were miscible with toluene, Et₂O, CH₂Cl₂, MeOH, tetrahydrofuran, acetone, DMF and DMSO in isochoric fusion test. The difference in miscibility with the least polar solvent (hexane) might be attributed to the polarity and repulsions between functional groups. However, the miscibility with water did not follow the same trend as shown in hexane, and this phenomenon is assumed to be the consequence of differences in the hydrophilicity of the functional groups. As we already discussed in the synthesis screening section, CH₃OCH₂CH₂- is highly hydrophilic while CF₃CH₂-group is hydrophobic. In this case, [ME, ME, ME] might be more suitable as a substitute for

DMPEG to dehydrate the gas stream, while [F, ME, F] can be utilized in different applications where moisture is not a consideration.

Table 8: Miscibility of compounds developed with common solvents.^a

Solvents	Hexane	Toluene	Et ₂ O	CH ₂ Cl ₂	MeOH
[E, K, E]	+	+	+	+	+
[ME, K, ME]	_	+	+	+	+
[F, K, F]	_	+	+	+	+
[ME, ME, ME]	_	+	+	+	+
[F, ME, F]	+	+	+	+	+
Solvents	THF	Water	Acetone	DMF	DMSO
[E, K, E]	+	_	+	+	+
[ME, K, ME]	+	+	+	+	+
[F, K, F]	+	_	+	+	+
[ME, ME, ME]	+	+	+	+	+
[F, ME, F]	+	_	+	+	+

a '+' = miscible and '-' = immiscible.

4. Conclusions

Three symmetric ketones ([E, K, E], [ME, K, ME] and [F, K, F]) and two triethers ([ME, ME, ME] and [F, ME, F]) based on a glycerol skeleton were synthesized and characterized for the first time. Density and viscosity data were obtained in a temperature range from T = 293.15 to 353.15 K. All the five compounds showed relatively low viscosity compared to DMPEG. Henry's constants were measured under modest pressure and then extrapolated in the range of 273.15 to 353.15 K with minor errors. [ME, ME, ME] and [F, ME, F] exhibited higher level of CO₂ capacity compared

to DMPEG and chosen ILs, indicating these two compounds good candidate as novel physical solvent for CO₂ capture. Electronic structure provided detailed energetic information about the absorption process. The five compounds showed consistency in good compatibility with common organic solvents except hexanes and the opposite hydrophilia nature of [ME, ME, ME] and [F, ME, F] may differentiate their applications in CO₂ removal process.

Supporting Information Available

¹H NMR spectra, density, viscosity and CO₂ solubility data for compounds studied in this work and simulation results are provided in supporting material.

Declaration of interest

The authors declare no conflict of interest.

Acknowledgements

Support from the National Science Foundation (EFMA-2029387) is gratefully acknowledged. Acknowledgment also is made to the Major Research Instrumentation (MRI) program of the NSF for the purchase of a NMR spectrometer (CHE-1919906) used in this work.

References

- 1. Quispe, C. A. G.; Coronado, C. J. R.; Carvalho Jr, J. A., Glycerol: Production, consumption, prices, characterization and new trends in combustion. *Renewable and Sustainable Energy Reviews* **2013**, *27*, 475-493.
- 2. Ayoub, M.; Abdullah, A. Z., Critical review on the current scenario and significance of crude glycerol resulting from biodiesel industry towards more sustainable renewable energy industry. *Renewable and Sustainable Energy Reviews* **2012**, *16* (5), 2671-2686.
- 3. Gatti, M.; Martelli, E.; Marechal, F.; Consonni, S., Review, modeling, Heat Integration, and improved schemes of Rectisol®-based processes for CO2 capture. *Applied Thermal Engineering* **2014**, *70* (2), 1123-1140.

- 4. Pakzad, P.; Mofarahi, M.; Ansarpour, M.; Afkhamipour, M.; Lee, C.-H., Chapter 3 CO2 absorption by common solvents. In *Advances in Carbon Capture*, Rahimpour, M. R.; Farsi, M.; Makarem, M. A., Eds. Woodhead Publishing: 2020; pp 51-87.
- 5. Ghasem, N., Chapter 21 CO2 removal from natural gas. In *Advances in Carbon Capture*, Rahimpour, M. R.; Farsi, M.; Makarem, M. A., Eds. Woodhead Publishing: 2020; pp 479-501.
- 6. Shukla, S. K.; Khokarale, S. G.; Bui, T. Q.; Mikkola, J.-P. T., Ionic Liquids: Potential Materials for Carbon Dioxide Capture and Utilization. *Frontiers in Materials* **2019**, *6* (42).
- 7. Aghaie, M.; Rezaei, N.; Zendehboudi, S., A systematic review on CO2 capture with ionic liquids: Current status and future prospects. *Renewable and Sustainable Energy Reviews* **2018**, *96*, 502-525.
- 8. Flowers, B. S.; Mittenthal, M. S.; Jenkins, A. H.; Wallace, D. A.; Whitley, J. W.; Dennis, G. P.; Wang, M.; Turner, C. H.; Emel'yanenko, V. N.; Verevkin, S. P.; Bara, J. E., 1,2,3-Trimethoxypropane: A Glycerol-Derived Physical Solvent for CO2 Absorption. *ACS Sustainable Chemistry & Engineering* **2017**, *5* (1), 911-921.
- 9. Qian, S.; Liu, X.; Dennis, G. P.; Turner, C. H.; Bara, J. E., Properties of symmetric 1,3-diethers based on glycerol skeletons for CO2 absorption. *Fluid Phase Equilibria* **2020**, *521*, 112718.
- 10. Qian, S.; Liu, X.; Emel'yanenko, V. N.; Sikorski, P.; Kammakakam, I.; Flowers, B. S.; Jones, T. A.; Turner, C. H.; Verevkin, S. P.; Bara, J. E., Synthesis and Properties of 1,2,3-Triethoxypropane: A Glycerol-Derived Green Solvent Candidate. *Industrial & Engineering Chemistry Research* **2020**, *59* (45), 20190-20200.
- 11. Scholz, E., Karl Fischer titrations of aldehydes and ketones. *Analytical Chemistry* **1985**, *57* (14), 2965-2971.
- 12. Bara, J. E.; Finotello, A.; Magee, J. W.; Qian, S.; O'Harra, K. E.; Dennis, G. P.; Noble, R. D., 110th Anniversary: Properties of Imidazolium-Based Ionic Liquids Bearing Both Benzylic and n-Alkyl Substituents. *Industrial & Engineering Chemistry Research* **2019**, *58* (38), 17956-17964.
- 13. Lee, C.; Yang, W.; Parr, R. G., Development of the Colle-Salvetti Correlation-Energy Formula into A Functional of the Electron Density. *Phys. Rev. B* **1988**, *37*, 785.
- 14. Becke, A. D., A New Mixing of Hartree–Fock and Local Density-Functional Theories. *J. Chem. Phys.* **1993**, *98*, 1372-1377.
- 15. Grimme, S.; Antony, J.; Ehrlich, S.; Krieg, H., A Consistent and Accurate ab initio Parametrization of Density Functional Dispersion Correction (DFT-D) for the 94 Elements H-Pu. *J. Chem. Phys.* **2010**, *132*, 154104.
- 16. Frisch, M.; Trucks, G.; Schlegel, H. B.; Scuseria, G. E.; Robb, M. A.; Cheeseman, J. R.; Scalmani, G.; Barone, V.; Mennucci, B.; Petersson, G., *et al.*, Gaussian 09, Revision D. 01, Gaussian. *Inc., Wallingford CT* **2009**.
- 17. Zhao, Y.; Truhlar, D. G., The M06 Suite of Density Functionals for Main Group Thermochemistry, Thermochemical Kinetics, Noncovalent Interactions, Excited States, and Transition Elements: Two New Functionals and Systematic Testing of Four M06-Class Functionals and 12 Other Functionals. *Theor. Chem. Acc.* **2008**, *120*, 215-241.
- 18. Lu, T.; Chen, F., Multiwfn: A Multifunctional Wavefunction Analyzer. *J. Comput. Chem.* **2012,** *33,* 580-592.
- 19. Lu, T.; Manzetti, S., Wavefunction and Reactivity Study of Benzo[a]pyrene Diol Epoxide and Its Enantiomeric Forms. *Struct. Chem.* **2014**, *25*, 1521-1533.
- 20. Lu, T.; Chen, F., Quantitative Analysis of Molecular Surface Based on Improved Marching Tetrahedra Algorithm. *J. Mol. Graph. Model.* **2012**, *38*, 314-323.
- 21. Murray, J. S.; Brinck, T.; Lane, P.; Paulsen, K.; Politzer, P., Statistically-Based Interaction Indices Derived from Molecular Surface Electrostatic Potentials: A General Interaction Properties Function (GIPF). *J. Mol. Struct. THEOCHEM* **1994**, *307*, 55-64.

- 22. Bader, R. F.; Carroll, M. T.; Cheeseman, J. R.; Chang, C., Properties of Atoms in Molecules: Atomic Volumes. *J. Am. Chem. Soc.* **1987**, *109*, 7968-7979.
- 23. Becke, A. D., Density-Functional Exchange-Energy Approximation with Correct Asymptotic Behavior. *Phys. Rev. A* **1988**, *38*, 3098.
- 24. Perdew, J. P., Density-Functional Approximation for the Correlation Energy of the Inhomogeneous Electron Gas. *Phys. Rev. B* **1986**, *33*, 8822.
- 25. Klamt, A., The COSMO and COSMO-RS solvation models. *Wiley Interdiscip. Rev.: Comput. Mol. Sci.* **2011**, *1*, 699-709.
- 26. Klamt, A.; Eckert, F.; Arlt, W., COSMO-RS: An Alternative to Simulation for Calculating Thermodynamic Properties of Liquid Mixtures. *Annu. Rev. Chem. Biomol. Eng.* **2010**, *1*, 101-122.
- 27. Liu, X.; O'Harra, K. E.; Bara, J. E.; Turner, C. H., Molecular Insight into the Anion Effect and Free Volume Effect of CO₂ Solubility in Multivalent Ionic Liquids. *Phys. Chem. Chem. Phys.* **2020**, *22*, 20618-20633.
- 28. Liu, X.; O'Harra, K. E.; Bara, J. E.; Turner, C. H., Solubility Behavior of CO2 in Ionic Liquids Based on Ionic Polarity Index Analyses. *The Journal of Physical Chemistry B* **2021**, *125* (14), 3665-3676.
- 29. Shannon, M. S.; Tedstone, J. M.; Danielsen, S. P.; Hindman, M. S.; Irvin, A. C.; Bara, J. E., Free Volume as the Basis of Gas Solubility and Selectivity in Imidazolium-Based Ionic Liquids. *Ind. Eng. Chem. Res.* **2012**, *51*, 5565-5576.
- 30. Lu, T., Molclus Program, Version 1.9.5. Beijing Kein Research Center for Natural Science, China. http://www.keinsci.com/research/molclus.html (accessed July 01st, 2020): 2016.
- 31. Pracht, P.; Bohle, F.; Grimme, S., Automated Exploration of the Low-Energy Chemical Space with Fast Quantum Chemical Methods. *Phys. Chem. Chem. Phys.* **2020**, *22*, 7169-7192.
- 32. Grimme, S.; Bannwarth, C.; Shushkov, P., A Robust and Accurate Tight-Binding Quantum Chemical Method for Structures, Vibrational Frequencies, and Noncovalent Interactions of Large Molecular Systems Parametrized for All spd-Block Elements (Z = 1–86). *J. Chem. Theory Comput.* **2017**, *13*, 1989-2009.
- 33. Pracht, P.; Caldeweyher, E.; Ehlert, S.; Grimme, S., A Robust Non-Self-Consistent Tight-Binding Quantum Chemistry Method for large Molecules. *ChemRxiv* **2019**, *preprint* (DOI: 10.26434/chemrxiv.8326202.v1).
- 34. Bannwarth, C.; Ehlert, S.; Grimme, S., GFN2-xTB—An Accurate and Broadly Parametrized Self-Consistent Tight-Binding Quantum Chemical Method with Multipole Electrostatics and Density-Dependent Dispersion Contributions. *J. Chem. Theory Comput.* **2019**, *15*, 1652-1671.
- 35. Brandenburg, J. G.; Bannwarth, C.; Hansen, A.; Grimme, S., B97-3c: A Revised Low-Cost Variant of the B97-D Density Functional Method. *J. Chem. Phys.* **2018**, *148*, 064104.
- 36. Neese, F., The ORCA Program System. Wiley Interdiscip. Rev.: Comput. Mol. Sci. 2012, 2, 73-78.
- 37. Neese, F., Software Update: the ORCA Program System, Version 4.0. *Wiley Interdiscip. Rev.: Comput. Mol. Sci.* **2018**, *8*, e1327.
- 38. Boys, S. F.; Bernardi, F., The Calculation of Small Molecular Interactions by the Differences of Separate Total Energies. Some Procedures with Reduced Errors. *Mol. Phys.* **1970**, *19*, 553-566.
- 39. Izgorodina, E. I.; Seeger, Z. L.; Scarborough, D. L. A.; Tan, S. Y. S., Quantum Chemical Methods for the Prediction of Energetic, Physical, and Spectroscopic Properties of Ionic Liquids. *Chem. Rev.* **2017**, *117*, 6696-6754.
- 40. Johnson, E. R.; Keinan, S.; Mori-Sánchez, P.; Contreras-García, J.; Cohen, A. J.; Yang, W., Revealing Noncovalent Interactions. *J. Am. Chem. Soc.* **2010**, *132*, 6498-6506.
- 41. Lefebvre, C.; Rubez, G.; Khartabil, H.; Boisson, J.-C.; Contreras-García, J.; Hénon, E., Accurately Extracting the Signature of Intermolecular Interactions Present in the NCI Plot of the Reduced Density Gradient versus Electron Density. *Phys. Chem. Chem. Phys.* **2017**, *19*, 17928-17936.

- 42. Humphrey, W.; Dalke, A.; Schulten, K., VMD: Visual Molecular Dynamics. *J. Mol. Graphics* **1996**, *14*, 33-38.
- 43. Li, J.; Mundhwa, M.; Henni, A., Volumetric Properties, Viscosities, Refractive Indices, and Surface Tensions for Aqueous Genosorb 1753 Solutions. *Journal of Chemical & Engineering Data* **2007**, *52* (3), 955-958.
- 44. Henni, A.; Tontiwachwuthikul, P.; Chakma, A., Solubilities of Carbon Dioxide in Polyethylene Glycol Ethers. *The Canadian Journal of Chemical Engineering* **2005**, *83* (2), 358-361.
- 45. Amaral, M.; Crespo, E. A.; Dariva, C.; Vega, L. F.; Carvalho, P. J.; Coutinho, J. A. P., High-pressure solubility of CO2 in glymes. *Fuel* **2018**, *219*, 120-125.
- 46. Finotello, A.; Bara, J. E.; Camper, D.; Noble, R. D., Room-Temperature Ionic Liquids: Temperature Dependence of Gas Solubility Selectivity. *Industrial & Engineering Chemistry Research* **2008**, *47* (10), 3453-3459.
- 47. Shiflett, M. B.; Yokozeki, A., Solubilities and Diffusivities of Carbon Dioxide in Ionic Liquids: [bmim][PF6] and [bmim][BF4]. *Industrial & Engineering Chemistry Research* **2005**, *44* (12), 4453-4464.
- 48. Wang, C.; Luo, X.; Luo, H.; Jiang, D.-e.; Li, H.; Dai, S., Tuning the Basicity of Ionic Liquids for Equimolar CO2 Capture. *Angewandte Chemie International Edition* **2011**, *50* (21), 4918-4922.
- 49. Chen, F.-F.; Huang, K.; Zhou, Y.; Tian, Z.-Q.; Zhu, X.; Tao, D.-J.; Jiang, D.-e.; Dai, S., Multi-Molar Absorption of CO2 by the Activation of Carboxylate Groups in Amino Acid Ionic Liquids. *Angewandte Chemie International Edition* **2016**, *55* (25), 7166-7170.
- 50. Liu, Z.; Lu, T.; Chen, Q., Intermolecular interaction characteristics of the all-carboatomic ring, cyclo[18]carbon: Focusing on molecular adsorption and stacking. *Carbon* **2021**, *171*, 514-523.